Applied Energy 169 (2016) 309–323

Contents lists available at ScienceDirect

Applied Energy

journal homepage: www.elsevier.com/locate/apenergy

Estimating hourly cooling load in commercial buildings using a thermal network model and electricity submetering data

Ying Ji, Peng Xu *, Pengfei Duan, Xing Lu

School of Mechanical Engineering, Tongji University, Shanghai 201804, China

HIGHLIGHTS

- Three hourly cooling load prediction models, called "RC-S" models, are proposed.
- Parameter optimization method with GA algorithm is proposed.
- Internal mass RC models compared to measured data are completed and analyzed.
- Internal mass RC models compared to EnergyPlus simulated data are done and analyzed.
- Better model is selected and it can provide reasonable estimation of cooling load.

ARTICLE INFO

Article history:
Received 7 September 2015
Received in revised form 4 February 2016
Accepted 5 February 2016

Keywords:
Cooling load estimation
Thermal network model
Electricity submetering data
GA algorithm
Parameter optimization

ABSTRACT

One major obstacle in Heating, Ventilation and Air Conditioning (HVAC) system Fault Detection and Diagnostics (FDD), retrofitting and energy performance evaluation is the lack of detailed hourly cooling load data. Cooling load measurement in commercial buildings is expensive and sometimes very difficult to implement. Detailed building simulation models, such as EnergyPlus, are too complicated to build and also must be calibrated. In this paper, an hourly cooling load prediction model, called the "RC-S" model, is proposed. This new cooling load calculation approach consists of a simplified thermal network model of the building envelope, a thermal network model for the building internal mass and the internal cooling load model from the submetering system. One existing RC model is introduced as reference model and three types of "RC-S" models are set up in this study. Genetic algorithm (GA) is selected to optimize the parameters in those models. Measurement data collected from a real commercial building and simulation data obtained from EnergyPlus model of the same commercial building are used to train and test the four models. The results prove that the proposed "RC-S" cooling load calculation method is more accurate than the existing RC model and much simpler than whole building simulation models. It can provide reasonable estimations of cooling loads for HVAC FDD and other performance evaluations.

1. Introduction

The building sector is a major consumer of energy worldwide and a large amount of energy is used for Heating, Ventilation and Air Conditioning (HVAC) [1–5]. One cause of high consumption in HVAC systems lies in their frequent failure to operate as intended after a period of operation, even with correct commissioning [6,7]. In many buildings, energy performance is not a concern as long as building comfort can be maintained. Many previous studies have focused on enhancing the operating efficiency of HVAC systems. These studies can be categorized by topic, such as Fault Detection and Diagnostics (FDD), supervisor optimal control, retrofit and continued commissioning. Reliable data on energy consumption and cooling loads form an indispensable basis for these functions.

In the last decade, interval metering and submetering of commercial building systems have become more popular in various countries and regions of the world. The energy meter structure is depicted in Fig. 1. Data on these meters are normally collected every 5–15 min, so over time, overwhelming amounts of data accumulate, providing a good platform for FDD and optimizing control for HVAC systems.

However, unlike electricity, few buildings have their cooling load metered. Cooling loads are typically measured using the supply and return temperatures and flow rates of chilled water. Cooling load measurement is not very expensive for a newly constructed system. However, it is often neglected because contractors' main concern is to meet the comfort requirements with

* Corresponding author. Tel.: +86 021 65989750.
E-mail address: xupeng@tongji.edu.cn (P. Xu).

http://dx.doi.org/10.1016/j.apenergy.2016.02.036
0306-2619/

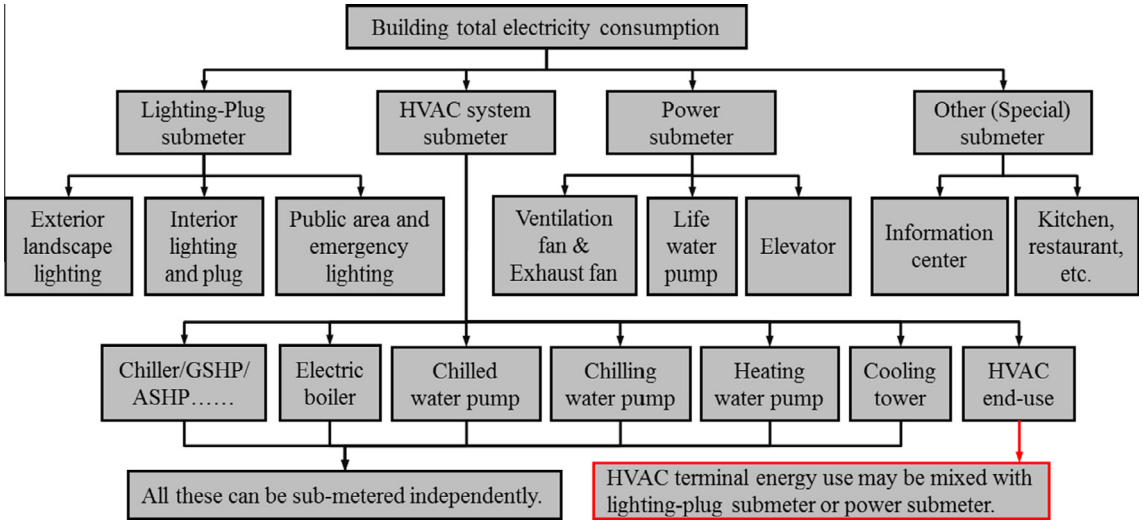

Fig. 1. Submetering system schematics and classification levels.

the lowest investment cost. In newly constructed buildings, the temperature and flow sensors are buried inside the chilled water pipe. The data are relatively accurate at the beginning, but sensors will drift and degrade over time. In existing buildings, it is necessary to drill holes to install sensors. Many building owners and operators forbid drilling into high-pressure pipes because of liability issues. In many cases, peeling off insulation and installing temperature and ultrasonic flow sensors attached to pipes is also prohibited.

In view of the importance of the cooling load and the difficulty of installing meters, an increasing number of scholars are dedicated to the study of calculating building loads with kinds of models. The paper is organized as follows. Section 2 is the literature review. Section 3 elaborates the previous RC model and three newly introduced models. This section also describes the principles of the parameter calibration process for the external building envelope and internal mass. Section 4 mainly describes the building information for the case study commercial building and its data acquisition. Section 5 is composed of three parts. Section 5.1 introduces the parameter calibration process for the external building envelope. Measured data and simulated data are utilized to compare and validate four models in Sections 5.2 and 5.3, respectively. Finally, the results from measured data and simulated data are further compared and summarized.

2. Literature review

In the 2001 ASHRAE Handbook—Fundamentals models are divided into two basic categories: 'forward modeling' and 'inverse modeling' [8]. Forward modeling generally begins with a physical description of a building. This includes the building's construction materials, lighting, equipment, occupants and the type of HVAC system. This type of model is typically used for designing a building and its HVAC system. Inverse models are derived from empirical historical data and are expressed in terms of one or more driving forces and a set of empirical parameters. A model form is predetermined and measured data are used to get the parameters that provide the most accurate representation for the chosen model form and data set. This type of model can be used for retrofit analysis, performance monitoring, FDD and on-line optimal control.

Forward models, also known as law-driven models, physical models or white box models, are the universally used method in the field of building load prediction. However, as mentioned above, the input parameters for these models are complicated and often are not available. It takes time and effort to establish and calibrate models, even for specialists with many years' experience, but the precision of the model still cannot be guaranteed [9–14]. Inverse modeling, also called data-driven modeling, can be generally classified into black and gray models. Black box models include traditional regression models [15–17], artificial neural network (ANN) models [18–21] and support vector machine (SVM) models [22–24] and so on. Black box models are trained and driven by a set of data. The training data set has stringent requirements on quality and time span. Furthermore, the training data are supposed to provide as much coverage of various conditions as possible. Many inverse models tend to have poor precision and weak robustness due to the lack of high-quality training data. Gray box models sit between white and black box models. Their approaches differ from black box approaches in that they use certain parameters identified from a physical system model. Examples of gray box models are decision tree models [25,26], Fourier series models [27–29] and thermal network models (RC model) [30]. Considering that the building loads have explicit components, RC models are more accurate because their parameters have obvious physical meanings and the models require less data than data-driven models. Therefore, RC models need less training and are more robust. Based on circuit principles and Kirchhoff electric current theory, a building thermal network model is presented as a simple simulation model of transient heat transfer through the building envelope and internal mass, which is called the "RC model". R is the thermal resistance of the material, and C is the heat capacity of materials.

The approaches to calculating the cooling load coming from a building envelope using RC models are detailed in a book written by Kreider and Rabl in the 1990s: 'Heating and Cooling of Buildings: Design for Efficiency' [30]. Braun and Chaturvedi [31] proposed an inverse gray thermal network model for transient building load prediction. Liao and Dexter [32] developed a gray second-order physical model to simulate the dynamic behavior of the existing heating system of a multi-zone residential building. Mitchell [33] postulated that the nodal placement of the 3R2C model could be obtained by matching the theoretical frequency response characteristics of the building envelope with the frequency response characteristics of the simplified model using a genetic algorithm. The numbers in front of R and C stand for the numbers of resistance and capacity factors in the model. Seem

et al. [34] indicated that the 3R2C model is very adaptable for modeling the external building envelope. Xu and Wang [35,36] compared the Conduction Transfer Function (CTF) model with the 3R2C model and validated the above viewpoint in Ref. [34]. Soon afterwards, Xu and Wang [37,38] proposed a simplified 2R2C model to consider the effect of the building internal mass on the cooling load using a genetic algorithm for the lumped parameters. However, the estimated cooling load deviates from the measured cooling load by 22%.

The two main reasons which cause the RC model bias are as follows: (1) Using the serial 2R2C model to describe the building internal mass is not accurate enough. In the 2R2C model, all internal mass, such as floors, internal walls and furniture, is seen as one entity. The model cannot reflect the effects on cooling load caused by the characteristics of different internal masses and the distribution differences of solar and internal radiation. (2) Researchers used the design power rate and schedule to estimate the internal cooling load from lighting and equipment in the previous study. However, in real building operation, the hourly power rate is very inconsistent with the design level.

Given these flaws, in this paper, a modified RC model for the building load forecasting, called the "RC-S" model, is presented. The S stands for submetering. The modeling of the external building envelope is same as in the conventional 3R2C model. However, to better describe the cooling load effects caused by the characteristics of different internal masses and radiation distribution differences, a parallel structure replaces the original serial model for describing the building internal mass. Submetering data rather than design data are used to estimate internal load and operating schedules. A case study of a commercial building in Shanghai is used to validate the proposed model and the result is promising.

3. Model descriptions

The principles of the RC models developed by Xu et al. [35–38] and the improved RC-S models are described here to introduce basic concepts of RC models. The RC model developed by Xu, Wang, et al. is denoted as 'model 0' and the improved models are denoted as 'model 1', 'model 2' and 'model 3', respectively.

3.1. Brief model introduction

3.1.1. Model 0

The structure of model 0 is illustrated in Fig. 2(a). The model gives a detailed description of the building external envelope and internal mass. Roofs and external walls are simplified as 3R2C models in the model 0. It should be noted that external walls are orientation-dependent due to different solar radiation at different solar angles. Internal mass (ceilings, internal walls, furniture, etc.) is described in a 2R2C series in the model. The parameters of 3R2C models of building envelopes can be determined by comparing the theoretical frequency response characteristics of building envelopes with the frequency response characteristics of the simplified model using a genetic algorithm, and the parameter optimization of the 2R2C model of the building internal mass is also optimized with a genetic algorithm by comparing the estimated cooling load with the actual cooling load. The estimated cooling load is calculated by following Eqs. (1)–(4) and (0-1)–(0-3).

$$C_{rf,1}\frac{dT_{rf,2}(t)}{dt}=\frac{T_{sol,rf}(t)-T_{rf,2}(t)}{R_{rf,1}}-\frac{T_{rf,2}(t)-T_{rf,4}(t)}{R_{rf,3}} \tag{1}$$

$$C_{rf,4}\frac{dT_{rf,4}(t)}{dt}=\frac{T_{rf,2}(t)-T_{rf,4}(t)}{R_{rf,3}}-\frac{T_{rf,4}(t)-T_{in}(t)}{R_{rf,5}} \tag{2}$$

$$C_{ei,2}\frac{dT_{ei,2}(t)}{dt}=\frac{T_{sol,ei}(t)-T_{ei,2}(t)}{R_{ei,1}}-\frac{T_{ei,2}(t)-T_{ei,4}(t)}{R_{ei,3}} \tag{3}$$

$$C_{ei,4}\frac{dT_{ei,4}(t)}{dt}=\frac{T_{ei,2}(t)-T_{ei,4}(t)}{R_{ei,3}}-\frac{T_{ei,4}(t)-T_{in}(t)}{R_{ei,5}} \tag{4}$$

$$C_{im,1}\frac{dT_{im,1}(t)}{dt}=Q_{r,1}-\frac{T_{im,1}(t)-T_{im,2}(t)}{R_{im,1}} \tag{0-1}$$

$$C_{im,2}\frac{dT_{im,2}(t)}{dt}=Q_{r,2}+\frac{T_{im,1}(t)-T_{im,2}(t)}{R_{im,1}}-\frac{T_{im,2}(t)-T_{in}(t)}{R_{im,2}} \tag{0-2}$$

$$\begin{aligned}Q_{est}=&\sum_{i=1}^{n}\left(\frac{T_{ei,4}(t)-T_{in}(t)}{R_{ei,5}}\right)+\frac{T_{rf,4}(t)-T_{in}(t)}{R_{rf,5}}\\&+\frac{T_{out}(t)-T_{in}(t)}{R_{win}}+\left(\frac{T_{im,2}(t)-T_{in}(t)}{R_{im,2}}\right)-C_{in}\frac{dT_{in}(t)}{dt}\\&+(Q_{conv}+Q_{fr}+Q_{la})\end{aligned} \tag{0-3}$$

where R and C are resistance and capacitance, respectively; T is temperature; and subscripts rf, im, ei, win and in indicate roof, internal mass, the ith external wall, window and inside, respectively. $Q_{r,1}$ and $Q_{r,2}$, absorbed by the nodes $C_{im,1}$ and $C_{im,2}$, respectively, are the radiation, including the solar radiation through windows, from occupants, lights, equipment, etc. Q_{conv} is the convective heat from occupants, lights, equipment, etc. Q_{fr} is the heat transfer due to fresh air induction and infiltration (exfiltration). Q_{la} is the latent heat gain from occupants, etc. Q_{est} is the estimated cooling load.

Following Sections 3.1.2–3.1.4 are the detailed descriptions of three improved models. The approach to modeling the external envelope in the improved models is the same as that in model 0. The main improvements are as follows: (1) Changing the model structure of the building internal mass (as shown in the dotted box in Fig. 2(a)), altering the form from series to parallel connections; and (2) Calculating the internal heat sources (occupants, lighting, equipment, etc.) from submetering data. Model 0 calculates the internal heat sources by referring to the design power in the relevant specification, while the modified models obtain real-time power consumption data from submetering systems, which is more reliable and accurate.

3.1.2. Model 1

The model is shown in Fig. 2(b). The model breaks the internal mass into several categories according to their level of thermal inertia, but not by the type of radiation these masses absorb. Thermal mass is classified into these three groups: (1) light thermal mass, which refers to carpet, light partitions, furniture, etc; (2) medium thermal mass, which refers to the furniture and internal walls with certain thicknesses; and (3) heavy thermal mass, represented by the thick floor slabs and weight-bearing walls. We assume that different types of internal mass absorb uniform radiation from glazing and internal heat sources. In other words, $Q_{r,11}$, $Q_{r,12}$ and $Q_{r,13}$ are all equal to one third of the total radiation. The estimated cooling load is calculated by following Eqs. (1)–(4) and (1-1)–(1-4).

$$C_{im,11}\frac{dT_{im,11}(t)}{dt}=Q_{r,11}-\frac{T_{im,11}(t)-T_{in}(t)}{R_{im,11}} \tag{1-1}$$

$$C_{im,12}\frac{dT_{im,12}(t)}{dt}=Q_{r,12}-\frac{T_{im,12}(t)-T_{in}(t)}{R_{im,12}} \tag{1-2}$$

$$C_{im,13}\frac{dT_{im,13}(t)}{dt}=Q_{r,13}-\frac{T_{im,13}(t)-T_{in}(t)}{R_{im,13}} \tag{1-3}$$

$$Q_{est} = \sum_{i=1}^{n}\left(\frac{T_{ei,4}(t)-T_{in}(t)}{R_{ei,5}}\right) + \frac{T_{rf,4}(t)-T_{in}(t)}{R_{rf,5}} + \frac{T_{out}(t)-T_{in}(t)}{R_{win}} + \left(\frac{T_{im,11}(t)-T_{in}(t)}{R_{im,11}} + \frac{T_{im,12}(t)-T_{in}(t)}{R_{im,12}} + \frac{T_{im,13}(t)-T_{in}(t)}{R_{im,13}}\right) - C_{in}\frac{dT_{in}(t)}{dt} + (Q_{conv} + Q_{fr} + Q_{la}) \quad (1\text{-}4)$$

3.1.3. Model 2

The model is shown in Fig. 2(c). The model breaks the internal mass into several categories according to the type of radiation it absorbs but not by the thermal mass level itself.

In Model 2, internal mass is also classified into the following three groups based on its received radiation: (1) thermal mass exposed to solar radiation, which is often represented by the floor, ceiling, furniture and decoration close to the external windows; (2) thermal mass which absorbs other radiation (from occupants, lights and equipment), which normally refers to most floors, internal walls and furniture in the building; and (3) thermal mass which is sheltered from any radiation, which refers to the floor slabs, internal walls and furniture in the shade. $Q_{r,21}$ is the solar radiation through windows and $Q_{r,22}$ is the total long-wave radiation from occupants, lights and equipment. We assume that the resistances and capacitances of internal mass are distributed evenly, that is, $R_{im,21} = R_{im,22} = R_{im,23}$, $C_{im,21} = C_{im,22} = C_{im,23}$. The estimated cooling load is calculated by following Eqs. (1)–(4) and (2-1)–(2-3).

$$C_{im,21}\frac{dT_{im,21}(t)}{dt} = Q_{r,21} - \frac{T_{im,21}(t)-T_{in}(t)}{R_{im,21}} \quad (2\text{-}1)$$

$$C_{im,22}\frac{dT_{im,22}(t)}{dt} = Q_{r,22} - \frac{T_{im,22}(t)-T_{in}(t)}{R_{im,22}} \quad (2\text{-}2)$$

$$Q_{est} = \sum_{i=1}^{n}\left(\frac{T_{ei,4}(t)-T_{in}(t)}{R_{ei,5}}\right) + \frac{T_{rf,4}(t)-T_{in}(t)}{R_{rf,5}} + \frac{T_{out}(t)-T_{in}(t)}{R_{win}} + \left(\frac{T_{im,21}(t)-T_{in}(t)}{R_{im,21}} + \frac{T_{im,22}(t)-T_{in}(t)}{R_{im,22}} + \frac{T_{im,23}(t)-T_{in}(t)}{R_{im,23}}\right) - C_{in}\frac{dT_{in}(t)}{dt} + (Q_{conv} + Q_{fr} + Q_{la}) \quad (2\text{-}3)$$

3.1.4. Model 3

The model is shown in Fig. 2(d), and it is the most complicated of the three improved models. Model 3 breaks the internal mass into several categories, taking into consideration both the thermal mass and the type of radiation it absorbs.

Internal mass is classified into two groups: light and heavy mass. A series–parallel hybrid structure is adopted which considers the temperature difference between the surface and internal space. Because different mass receives different solar radiation, the following assumptions are made: (1) only a small portion of direct solar radiation heat through windows lands on the heavy internal mass; and (2) Other long-wave radiation is radiated onto the heavy and light thermal mass. The above hypotheses can be expressed by the following equations: $R_{im,31} = R_{im,33} \neq R_{im,35}$, $R_{im,32} = R_{im,34} \neq R_{im,36}$, $C_{im,31} = C_{im,33} \neq C_{im,35}$, $C_{im,32} = C_{im,34} \neq C_{im,36}$. $Q_{r,31}$ is the solar radiation from glazing. $Q_{r,32}$ and $Q_{r,33}$ are both equal to half of the total long-wave radiation. The estimated cooling load is calculated by following Eqs. (1)–(4) and (3-1)–(3-7).

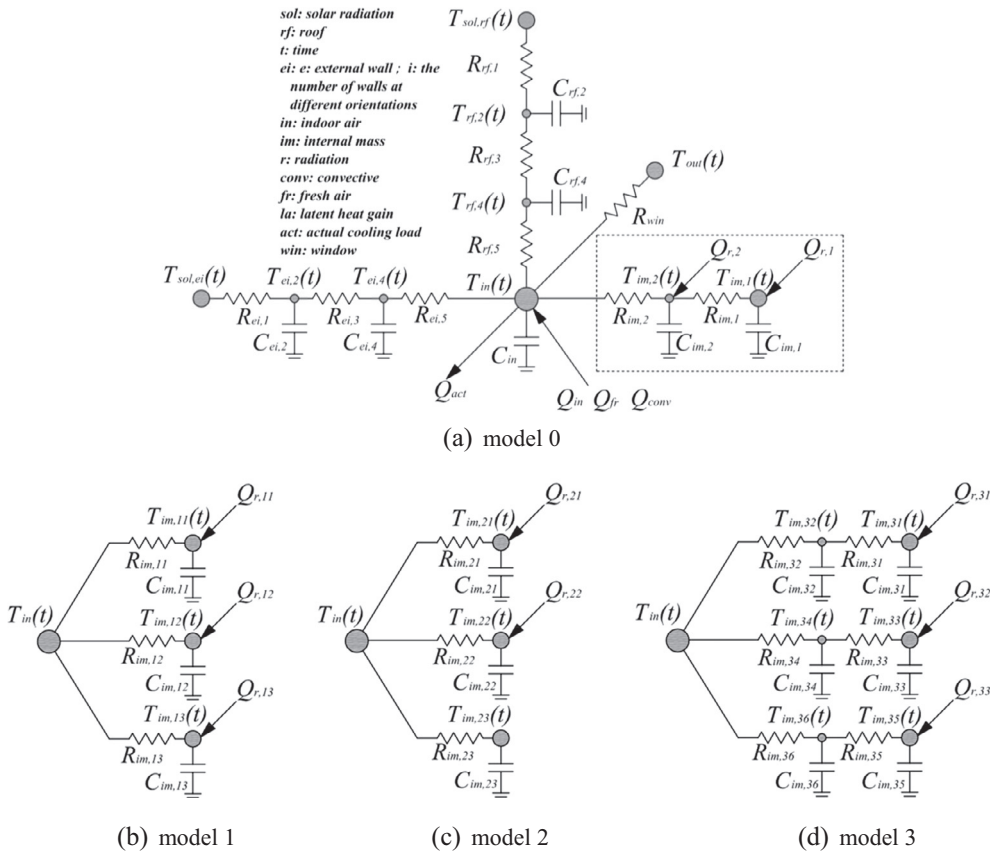

Fig. 2. Schematics of the simplified building cooling/heating load model.

$$C_{im,31}\frac{dT_{im,31}(t)}{dt} = Q_{r,31} - \frac{T_{im,31}(t) - T_{im,32}(t)}{R_{im,31}} \tag{3-1}$$

$$C_{im,33}\frac{dT_{im,33}(t)}{dt} = Q_{r,32} - \frac{T_{im,33}(t) - T_{im,34}(t)}{R_{im,33}} \tag{3-2}$$

$$C_{im,35}\frac{dT_{im,35}(t)}{dt} = Q_{r,33} - \frac{T_{im,35}(t) - T_{im,36}(t)}{R_{im,35}} \tag{3-3}$$

$$C_{im,32}\frac{dT_{im,32}(t)}{dt} = \frac{T_{im,31}(t) - T_{im,32}(t)}{R_{im,31}} - \frac{T_{im,32}(t) - T_{in}(t)}{R_{im,32}} \tag{3-4}$$

$$C_{im,34}\frac{dT_{im,34}(t)}{dt} = \frac{T_{im,33}(t) - T_{im,34}(t)}{R_{im,33}} - \frac{T_{im,34}(t) - T_{in}(t)}{R_{im,34}} \tag{3-5}$$

$$C_{im,36}\frac{dT_{im,36}(t)}{dt} = \frac{T_{im,35}(t) - T_{im,36}(t)}{R_{im,35}} - \frac{T_{im,36}(t) - T_{in}(t)}{R_{im,36}} \tag{3-6}$$

$$\begin{aligned} Q_{est} = {} & \sum_{i=1}^{n}\left(\frac{T_{ei,4}(t) - T_{in}(t)}{R_{ei,5}}\right) + \frac{T_{rf,4}(t) - T_{in}(t)}{R_{rf,5}} + \frac{T_{out}(t) - T_{in}(t)}{R_{win}} \\ & + \left(\frac{T_{im,32}(t) - T_{in}(t)}{R_{im,32}} + \frac{T_{im,34}(t) - T_{in}(t)}{R_{im,34}} + \frac{T_{im,36}(t) - T_{in}(t)}{R_{im,36}}\right) \\ & - C_{in}\frac{dT_{in}(t)}{dt} + (Q_{conv} + Q_{fr} + Q_{la}) \end{aligned} \tag{3-7}$$

3.2. Optimizing models of the building envelope

The aim of optimizing models for calculating cooling load through the building envelope is to search the most suitable parameters for describing the frequency and phase lag characteristics and to find the one that best matches with the physical model. The optimization process can be divided into three steps: (1) deduce the equivalent frequency characteristics of the physical model; (2) deduce the equivalent frequency characteristics of the simplified 3R2C model; and (3) calculate the parameters of 3R2C models of the building envelope using a genetic algorithm (GA), ensuring the frequency characteristics of the two models are as identical as possible.

3.2.1. Frequency characteristics of the physical model

The procedure for deducing the transmission matrix of heat transfer for one-dimensional homogeneous multilayer plane constructions in the Laplace domain has been studied by many researchers [38–41]. In this paper, the deduction process is only summarized, instead of detailed.

Heat transfer through the building envelope is generally regarded as a one-dimensional process, the model can be expressed as the transmission Eq. (5) in terms of Laplace variable s.

$$\begin{bmatrix} T_{in}(s) \\ q_{in}(s) \end{bmatrix} = M(s)\begin{bmatrix} T_{out}(s) \\ q_{out}(s) \end{bmatrix} = \begin{bmatrix} A(s) & B(s) \\ C(s) & D(s) \end{bmatrix}\begin{bmatrix} T_{out}(s) \\ q_{out}(s) \end{bmatrix} \tag{5}$$

where T is temperature, q is heat flow, and $M(s)$ is the total transmission matrix of the entire wall as well as the products of individual layer transmission matrices, including the surface films on both sides. Thus, $M(s)$ can also be expressed as Eq. (6) and $A(s)$, $B(s)$, etc. are the elements in the matrix. In other words, we use matrix format to express the heat transfer equations and actually the $A(s)$, $B(s)$, etc. are the coefficients of equations.

$$M(s) = \begin{bmatrix} A(s) & B(s) \\ C(s) & D(s) \end{bmatrix} = M_{in}(s)M_n(s)\ldots M_1(s)M_{out}(s) \tag{6}$$

$$\text{where } M_i(s) = \begin{bmatrix} A_i(s) & B_i(s) \\ C_i(s) & D_i(s) \end{bmatrix} \quad (i = 1, 2, 3\ldots) \tag{7}$$

Because Eq. (5) has a unique solution, there exists $A(s)D(s) - B(s)C(s) = 0$. Eq. (5) can thus be transformed into Eq. (8).

$$\begin{aligned} \begin{bmatrix} q_{out}(s) \\ q_{in}(s) \end{bmatrix} &= \begin{bmatrix} -A(s)/B(s) & 1/B(s) \\ -1/B(s) & D(s)/B(s) \end{bmatrix}\begin{bmatrix} T_{out}(s) \\ T_{in}(s) \end{bmatrix} \\ &= \begin{bmatrix} -G_X(s) & G_Y(s) \\ -G_Y(s) & G_Z(s) \end{bmatrix}\begin{bmatrix} T_{out}(s) \\ T_{in}(s) \end{bmatrix} \end{aligned} \tag{8}$$

$$\text{where } G_X(s) = A(s)/B(s) \tag{9}$$

$$G_Y(s) = 1/B(s) \tag{10}$$

$$G_Z(s) = D(s)/B(s) \tag{11}$$

Substituting s with $j\omega(j = \sqrt{-1})$ in Eqs. (9)–(11) gives complex functions $G_X(j\omega)$, $G_Y(j\omega)$ and $G_Z(j\omega)$, which are the frequency characteristics of the external, cross and internal heat conduction of the theoretical building envelope model, respectively [42]. These frequency characteristics are represented by the amplitudes and phase lags of these three complex functions representing the theoretical frequency characteristics of the external, cross and internal heat conduction.

3.2.2. Frequency characteristics of the 3R2C model

The simplified 3R2C model resembles the theoretical model, with the same transfer model. The only difference is that the nRnC theoretical model is simplified to five elements (three resistances and two capacitances). The 3R2C model can be represented by Eq. (12).

$$\begin{aligned} \begin{bmatrix} q_{out}(s) \\ q_{in}(s) \end{bmatrix} &= \begin{bmatrix} -A'(s)/B'(s) & 1/B'(s) \\ -1/B'(s) & D'(s)/B'(s) \end{bmatrix}\begin{bmatrix} T_{out}(s) \\ T_{in}(s) \end{bmatrix} \\ &= \begin{bmatrix} -G'_X(s) & G'_Y(s) \\ -G'_Y(s) & G'_Z(s) \end{bmatrix}\begin{bmatrix} T_{out}(s) \\ T_{in}(s) \end{bmatrix} \end{aligned} \tag{12}$$

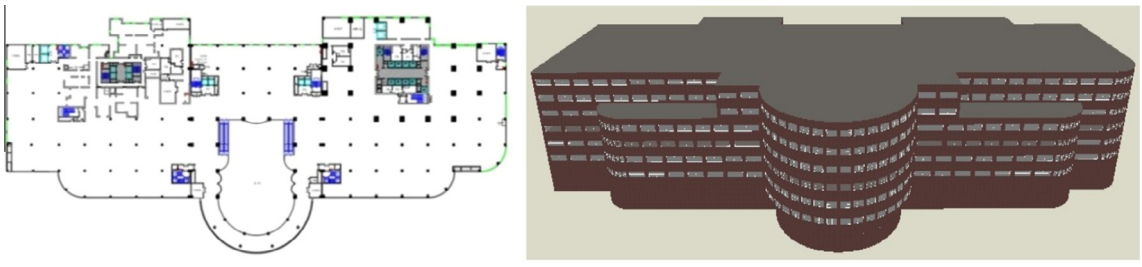

(a) (b)

Fig. 3. The plan drawing (a) and outline drawing (b) of the building analyzed in this paper.

where $G'_X(s) = A'(s)/B'(s)$ (13)

$G'_Y(s) = 1/B'(s)$ (14)

$G'_Z(s) = D'(s)/B'(s)$ (15)

Substituting s with $j\omega\left(j=\sqrt{-1}\right)$ in Eqs. (13)–(15) yields complex functions $G'_X(j\omega)$, $G'_Y(j\omega)$ and $G'_Z(j\omega)$, which are the frequency characteristics of the external, cross and internal heat conduction of the simplified 3R2C model, respectively [42]. These frequency characteristics are also represented by the amplitudes and phase lags of these three complex functions of the 3R2C model, which are compared with the theoretical frequency characteristics to optimize the theoretical parameters.

3.2.3. Objective function of parameter optimization

The optimization is actually searching for optimal parameters which allow the simplified 3R2C model to behave as similarly to the theoretical physical model as possible. The objective function of the simplified 3R2C model is expressed in Eq. (16).

$$J_{3R2C}(R_1,R_5,C_4) = \sum_{n=1}^{N}\sum_{m=X,Y,Z}\left(W_m^{AM}\left||G_m(j\omega_n)| - |G'_m(j\omega_n)|\right| + W_m^{PL}\left|PL(G_m(j\omega_n)) - PL(G'_m(j\omega_n))\right|\right) \quad (16)$$

where PL is the phase lag, AM is the amplitude, N is the number of frequency points, and W is the weighting factor associated with the amplitudes and phase lags of frequency characteristics of the external, cross and internal heat conduction, respectively. In this study, all of the weighting factors were set to 1, as it was found that this value works well. The parameter optimization constraints are listed in Eq. (17). R and C represent the total thermal resistance and thermal capacitance, respectively. The specific values should be calculated according to the data of the actual case.

$$\begin{cases} 0 < R_1 < R \\ 0 < R_5 < R \\ 0 < R_1 + R_5 < R \\ R_3 = R - R_1 - R_5 \\ 0 < C_4 < C \\ C_2 = C - C_4 \end{cases} \quad (17)$$

N is the number of frequency points. And the frequency range $(10^{-n_1}, 10^{-n_2})$ is determined as follows. n_1, n_2 and N are generally chosen as 8, 3 and 10 $(n_1 - n_2) + 1$, respectively [43]. The use of a GA estimator to optimize the parameters is described in detail in Section 5.

Table 1
Submeters summary of the building studied in this paper.

Main submeters	Directly measured	Secondary submeters	Directly measured	Source of building cooling/heating load
Lighting-plug submeter	**Yes**	Lighting and plug	No	Yes
		Exterior landscape lighting	**Yes**	No
		corridor and public area lighting	No	Yes
HVAC submeter	No	Terminal units	Yes	Yes
		HVAC Plant	Yes	No
Power submeter	**Yes**	Elevator	**Yes**	No (motor is on the roof)
		Non-HVAC water pump	No	Yes
		Ventilation/Exhaust fan	No	Yes
Others/Specials	**Yes**	Information center	Yes	Independent air-conditioning

Table 2
Material layers of the building envelope and main internal structures.

Envelope	Layers	Thickness (mm)	Conductivity (W/m °C)	Density (kg/m^3)	Specific heat (J/kg °C)
Roof	Insulation mortar	20	0.08	400	1045.8
	Expanded perlite	50	0.16	400	1170
	Reinforced concrete	200	1.74	2500	920
	Cement mortar screeding	30	0.93	1800	1050
	Lime mortar	20	0.81	1600	1050
External wall	Granite	20	3.49	2800	920
	Insulation mortar	20	0.08	400	1045.8
	Cement mortar screeding	30	0.93	1800	1050
	Concrete block	200	0.68	1300	537.8
	Lime mortar	30	0.81	1600	1050
External window	Ordinary glass	3			
	Air space	6			
	Ordinary glass	3			
Ground floor	Cement base insulation mortar	300	0.085	450	1164.8
	Reinforced concrete	500	1.74	2500	920
	Cement mortar screeding	30	0.93	1800	1050
Internal structures	Layers	Thickness (mm)	Conductivity (W/m °C)	Density (kg/m^3)	Specific heat (J/kg °C)
Internal floor	Lime mortar	30	0.81	1600	1050
	Insulation mortar	20	0.08	400	1045.8
	Reinforced concrete	120	1.74	2500	920
	Lime mortar	30	0.81	1600	1050
Internal wall	Lime mortar	30	0.81	1600	1050
	Reinforced concrete	120	1.74	2500	920
	Lime mortar	30	0.81	1600	1050

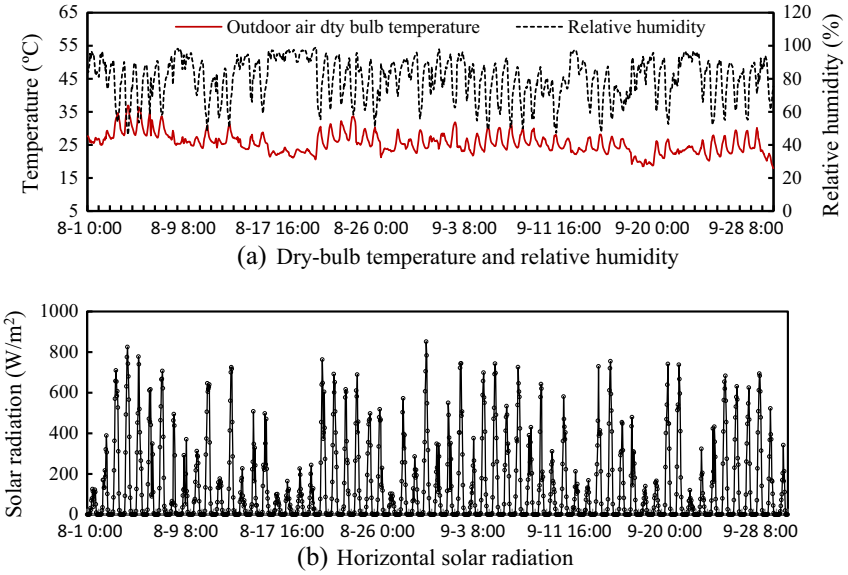

Fig. 4. Weather data for Shanghai from May 2014 to October 2014.

3.3. Optimized model of building internal mass

The parameter optimization of the building internal mass is relatively easy to implement. The objective is to minimize the integrated root-mean-square error of the predicted load, as defined in Eq. (18).

$$J_{RC}(C_{im,1}, R_{im,1}, \ldots C_{im,2}, R_{im,2}, \ldots) = \sqrt{\frac{\sum_{k=1}^{N}(Q_{act,k} - Q_{est,k})^2}{N-1}} \quad (18)$$

where Q_{act} and Q_{est} are the actual measured and estimated cooling loads, respectively, and $C_{im,1}$, $R_{im,1}$, etc. are the parameters of the internal mass model, whose numbers are determined by the specified model.

It is also worth noting that a genetic algorithm (GA) is employed as the parameter optimization method to identify a sufficiently good solution. There have been massive books and research articles on the principle and application of GA, so it will not be described in detail in this paper.

Different from the complex optimization process of the building envelope and internal mass, the internal heat gains are very easy to calculate according to standards without complex models. It will be calculated in detail in the next case study section.

4. Case study

4.1. Building description

Located in the Shanghai urban area, the target building is a multi-function commercial building with eight floors from the second floor underground (B2) to the sixth floor above ground (F6). The second floor underground is not air conditioned and is used for the HVAC plant and some facility rooms. The first floor underground to the fourth floor serves as a shopping mall. The open hours are from 9:00 a.m. to 22:00 p.m. The fifth and sixth floors are office zones. Work hours are from 8:00 a.m. to 17:00 p.m. The total building area of building A is approximately 68,000 m^2 and the story height is 4.5 m. Building A covers an area of 9112 m^2 in an irregular shape with a length of 153 m. The window to wall ratio of each façade is 18% (east), 40% (south), 18% (west) and 10% (north). The plan and outline drawings are shown in Fig. 3. After an on-site survey, the detailed submeter data are summarized in Table 1. The main HVAC equipment for this building is located on the second floor underground. The cooling tower is on the roof and AHUs are on each floor serviced.

The material layers of the building envelope and main internal structures are summarized in Table 2.

4.2. Data acquisition

4.2.1. Weather data

To obtain real-time weather data, a small weather station was built and data acquisition began in April 2014. The record frequency is 10 min. The collected data include outdoor air dry-bulb temperature, relative humidity, horizontal solar radiation, wind speed and wind direction. Among these parameters, the outdoor air dry-bulb temperature, relative humidity and horizontal solar radiation are more critical than the others. Just the data in August and September are used in this paper and shown in Fig. 4.

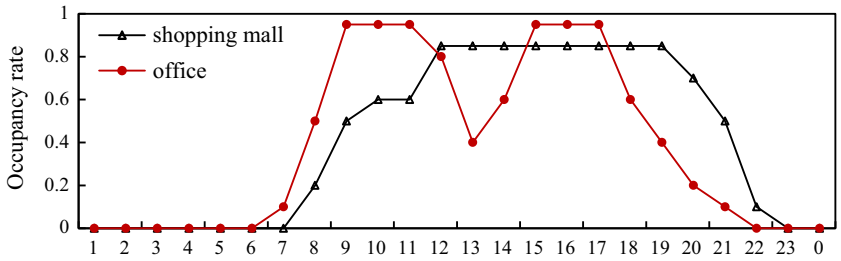

Fig. 5. Normal patterns of the occupancy load profile.

Table 3
Input data for the estimation of the building internal mass.

Internal mass	Layers	Thickness (mm)	Conductivity (W/m °C)	Density (kg/m3)	Specific heat (J/kg °C)
Decoration 1	Wood 1	10	0.29	500	2510
Decoration 2	Wood 2	20	0.23	600	1890
Decoration 3	Fiberboard	50	0.29	500	2510

4.2.2. On-site data

The solar air temperatures of external walls and roofs at different orientations are site-measured and the wall temperature is calculated by taking an average of temperature sensors attached to the external walls. The indoor air temperature is also determined in Eq. (19) as the weighted average of the temperature at different spatial locations.

$$\overline{T} = \frac{\sum_{i=1}^{n} T_i V_i}{\sum_{i=1}^{n} V_i} \tag{19}$$

where $\overline{T}$ is the indoor mean temperature, T_i is the temperature of the ith measurement point, and V_i is the volume of space i, n is the total number of the spaces.

The lighting and equipment power intensity are directly retrieved from the submetering system; the hourly power consumption is treated as the power intensity over that period. If the power consumption of a lighting-plug submeter is measured at 800 kW/h, the lighting and equipment power intensity can be considered to be 800 kW for that hour. Referring to the ASHRAE Handbook [44], convective and radiant heat from lighting and equipment power were found to account for 80% and 20% separately.

There is no automatic occupancy counting system in building A. The on-site survey concluded that the peak occupant density of the office area is 8 m^2/person on workdays and that of the shopping area is 6 m^2/person. The schedules are shown in Fig. 5. Latent heat, convective heat and radiant heat contribute 40%, 20% and 40% of occupancy heat gains, respectively [44].

It can be inferred from the literature [45–47] that the modern commercial building is sufficiently tight and the infiltration airflow may be even as low as 0.1–0.3 ac/h for some tightly enclosed buildings. The shape coefficient and window to wall ratio of this building are both relatively small, and the building is well constructed. Thus, an air change of 0.1 ac/h is used in this model. It is recommended to set the outdoor air rate based on the actual HVAC system. In this HVAC system, one AHU serves as a fresh air unit on each floor and has a fixed outdoor air rate of approximately 1 ac/h, so the outdoor air rate in this model is also set to 1 ac/h.

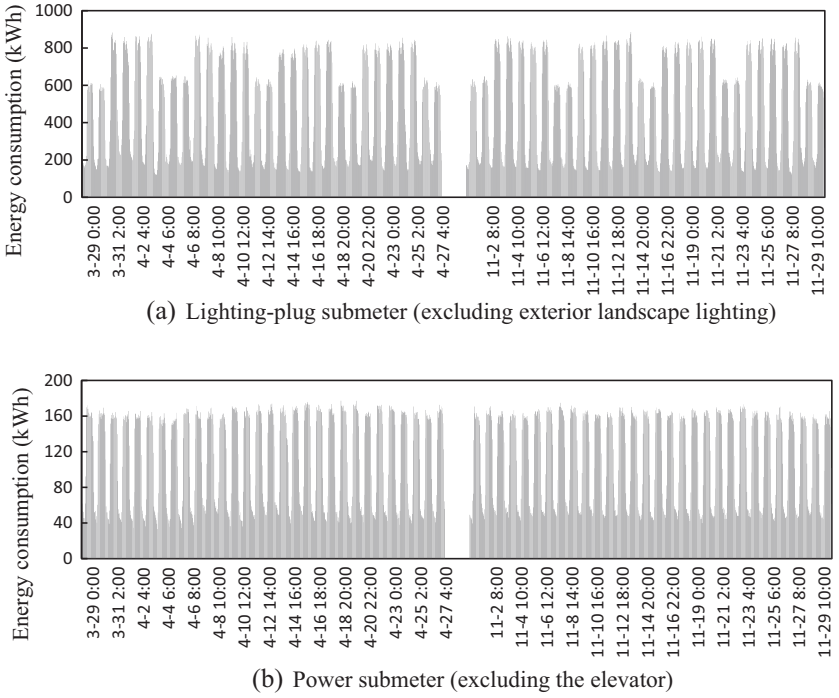

Fig. 6. Selected lighting-plug and power submeter data to train and validate Fourier series models.

Table 4
Results of the training and validation model of each submeter analyzed in this study.

Submeters	Day type	Training model R^2	Training model CV (%)	Training model MRE (%)	Validating model CV (%)	Validating model MRE (%)
Lighting-plug submeter (excluding exterior landscape lighting)	Workday	0.9850	6.529	4.772	4.518	4.255
	Non-workingday	0.9836	6.357	4.433	3.074	3.825
Power submeter (excluding elevator)	Full year	0.9745	7.479	4.685	5.482	4.082

The cooling load can be calculated indirectly by measuring the supply and return temperatures as well as the flow rate of the chilled water trunk, as expressed in Eq. (20).

$$\text{Hourly cooling load} = \sum_{1}^{60/t}\left(CM_j\Delta T_j \times \frac{60}{t}\right) \quad (20)$$

where t is the data collection cycle of temperature and water flow rate (min). C is the specific heat of water (4.187 kJ/(kg °C)). M_j is the chilled water flow rate (kg/s). ΔT_j is the temperature difference between the chilled water (hot water) inlet and outlet (°C).

Table 5
Schedules set in the building energy simulation model of the building.

Submeters	Lighting-plug submeter				Power submeter
	Lighting-plug submeter of office area in workdays	Lighting-plug submeter of shopping area	Night lighting in workdays	Night lighting in non-workdays	Power submeter (excluding elevator)
Peak (kW)	227	628	303		166
Area (m^2)	18,000	45,000	63,000	63,000	63,000
Density (W)	12.61	13.96	4.81	4.81	2.63
1:00	0.00	0.00	0.63	0.66	0.33
2:00	0.00	0.00	0.58	0.63	0.31
3:00	0.00	0.00	0.56	0.58	0.29
4:00	0.00	0.00	0.54	0.54	0.28
5:00	0.00	0.00	0.54	0.54	0.27
6:00	0.00	0.00	0.68	0.60	0.25
7:00	0.35	0.32	0.00	0.00	0.33
8:00	0.63	0.37	0.00	0.00	0.48
9:00	0.77	0.76	0.00	0.00	0.87
10:00	0.89	0.95	0.00	0.00	1.00
11:00	0.92	0.96	0.00	0.00	0.99
12:00	1.00	0.96	0.00	0.00	0.98
13:00	0.82	1.00	0.00	0.00	0.98
14:00	0.72	0.99	0.00	0.00	0.99
15:00	0.78	0.94	0.00	0.00	1.00
16:00	0.83	0.97	0.00	0.00	0.99
17:00	0.88	0.98	0.00	0.00	0.99
18:00	0.96	0.97	0.00	0.00	0.98
19:00	0.90	0.97	0.00	0.00	0.99
20:00	0.78	0.96	0.00	0.00	0.98
21:00	0.65	0.89	0.00	0.00	0.91
22:00	0.54	0.57	0.00	0.00	0.67
23:00	0.00	0.00	1.00	0.78	0.42
0:00	0.00	0.00	0.75	0.72	0.36

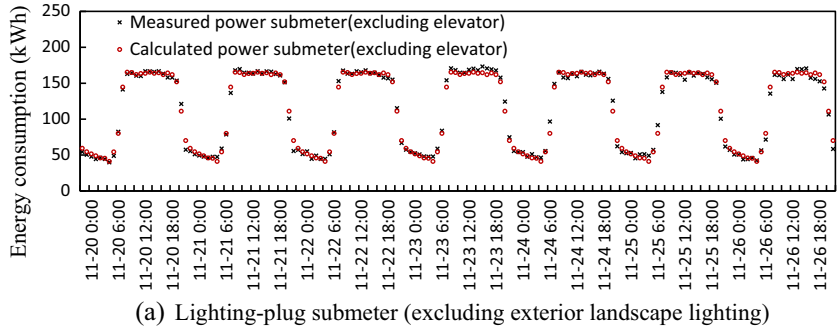

(a) Lighting-plug submeter (excluding exterior landscape lighting)

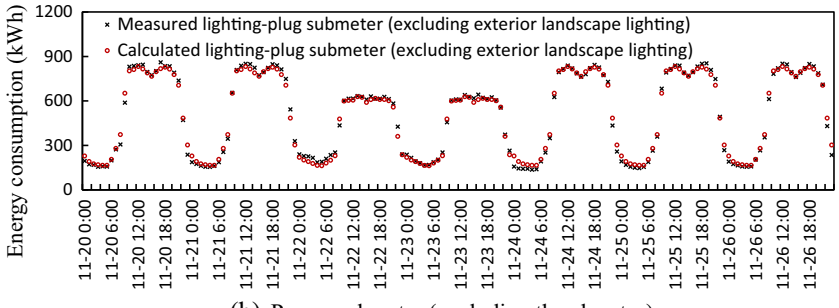

(b) Power submeter (excluding the elevator)

Fig. 7. Comparison of measured submeters and simulated submeters for one week.

4.2.3. Physical model simulated data [49]

The comparison of four models is conducted using both testing data and physical model simulated data. EnergyPlus is used to establish the physical model and a set of complete EnergyPlus simulated data is used for calculations in Section 5.

The target building covers an area of 9,112 m^2 in an irregular shape (see Fig. 3). To simply the model, the building geometry is changed to rectangular (152 m × 60 m) but the building area is left unchanged, and the height is the same as that of the real building. In the real building, there are four AHUs on each floor, so each floor of the model is divided into four zones. The weather parameters in the simulation model are set according to the acquired data mentioned in Section 4.2.1. The settings for the building envelope are based on Table 2 and lumped data, while Table 3 is used for the building internal mass inputs. The occupant, infiltration airflow and fresh air volume inputs are set as described in Section 4.2.2.

A physical model needs accurate inputs for the lighting and equipment schedule. Refs. [29,48,49] declared that lighting and equipment energy use varies periodically in daily and annual cycles. These energy uses are independent of ambient temperature and other weather variables in commercial buildings and can therefore be expressed by a Fourier series model. For normal commercial buildings, a Fourier series model with variable '*h*' can adequately reveal the power consumption characteristics of the lighting and equipment (Eq. (21)). Day types must be separated into working days and non-working days for the office building, but the separation is unnecessary in shopping and retail buildings.

$$E_L(E_P) = a + \sum_{n=1}^{n_{max}} [\delta_n \sin(2\pi\omega_n)h + \eta_n \cos(2\pi\omega_n)h] + \varepsilon, \quad \omega_n = \frac{n}{24}, \; n = 1 \sim 12 \tag{21}$$

Using the above Fourier series model, we can calculate the hourly submeter in each day type. Under the same day type, the maximum hourly energy consumption at each submeter is chosen as the set point and the ratio of the value of other time to the maximum value is calculated as a fraction of the schedule. The proportions of convection and radiation heat from lamps and equipment are standard values in the ASHRAE Handbook [44].

According to Table 1, it is not difficult to find that there are only two types of submeters contributing to the cooling load. They are (1) lighting-plug submeters (excluding exterior landscape lighting), and (2) power submeters (excluding the elevator). Submeters in transition seasons are selected to train and validate the Fourier series model (Eq. (21)). The spring training data from March 29th, 2014, to April 27th, 2014, and fall validation data from November 1st, 2014, to November 30th, 2014, are illustrated in Fig. 6.

The training and validation results of each model, listed in Table 4, are quite satisfactory. All R^2 of the training models are larger than 0.95. The best result is generated by lighting-plug submeters (excluding exterior landscape lighting) on non-workdays, with a CV (coefficient of variation) of 3.074% and MRE (mean relative error) of 3.825%.

Using the calculation, we can estimate the hourly electricity consumption and maximum value of each submeter. After the above work, the model setting becomes very simple. The maximum electricity consumption data for each submeter is chosen as the design value and the ratio of the value at any other hour to the peak value is calculated as the schedule factor. Using this method, the schedules for this case are listed in Table 5 and the comparison of measured submeters and simulated submeters for one week is illustrated in Fig. 7.

This section includes a detailed description of an objective building and the data acquisition process from on-site investigation and field testing. An EnergyPlus model is set up to provide simulated data for the parameter identification process discussed in Section 3.

Table 6
Details of actual external walls and roof of the building studied in this paper.

Envelope	Layers	Thickness (mm)	Conductivity (W/m °C)	Density (kg/m3)	Specific heat (J/kg °C)	R (m^2 k/W)	C (J/m^2 K)
Roof	Outside surface film	–	–	–	–	0.0400	–
	Insulation mortar	20	0.08	400	1045.8	0.2500	8366
	Expanded perlite	50	0.16	400	1170	0.3125	23,400
	Reinforced concrete	200	1.74	2500	920	0.1149	460,000
	Cement mortar screeding	30	0.93	1800	1050	0.0323	56,700
	Lime mortar	20	0.81	1600	1050	0.0247	33,600
	Inside surface film	–	–	–	–	0.1150	–
Total						0.8894	582,066
External wall	Outside surface film	–	–	–	–	0.0400	–
	Granite	20	3.49	2800	920	0.0057	51,520
	Insulation mortar	20	0.08	400	1045.8	0.2500	8366
	Cement mortar screeding	30	0.93	1800	1050	0.0323	56,700
	Concrete block	200	0.68	1300	537.8	0.2941	139,828
	Lime mortar	30	0.81	1600	1050	0.0370	50,400
	Inside surface film	–	–	–	–	0.1150	–
Total						0.7741	306,814

Table 7
Parameters of simplified 3R2C models of external wall and roof.

Envelope	Model	Parameters of resistance and capacitance R (m^2 k/W), C (J/m^2 K)						
		R1	C2	R3	C4	R5	Rt	Ct
Roof	Theoretical model	–	–	–	–	–	0.8894	582,066
	Optimal model	0.4640	40,066	0.2685	542,000	0.1569	0.8894	582,066
External wall	Theoretical model	–	–	–	–	–	0.7741	306,814
	Optimal model	0.0496	59,014	0.5862	247,800	0.1383	0.7741	306,814

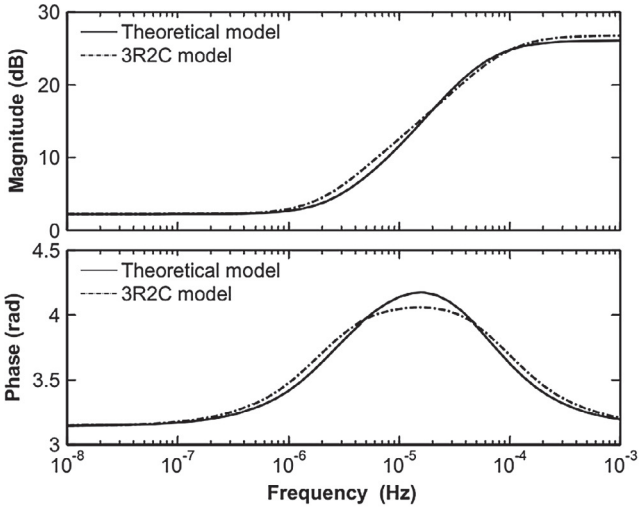

(a) External heat conduction

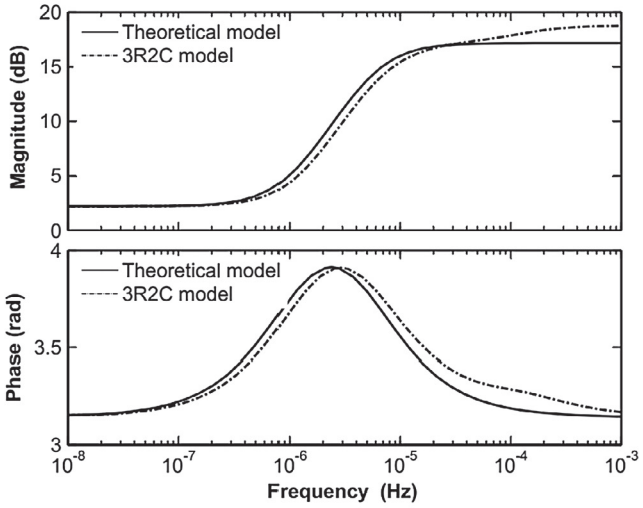

(b) Cross heat conduction

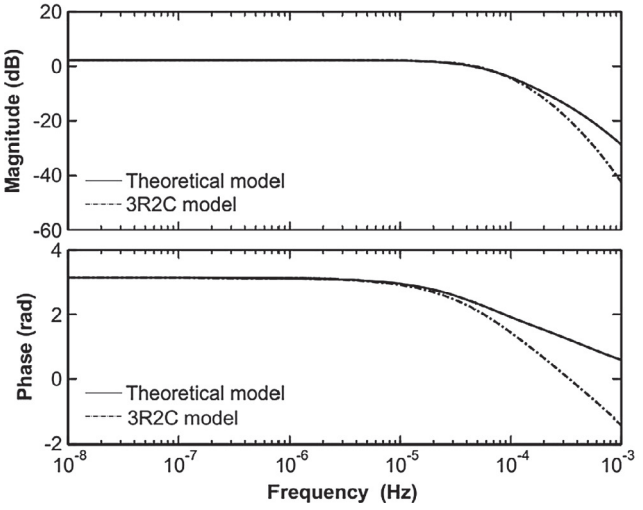

(c) Internal heat conduction

Fig. 8. Bode diagrams of external wall.

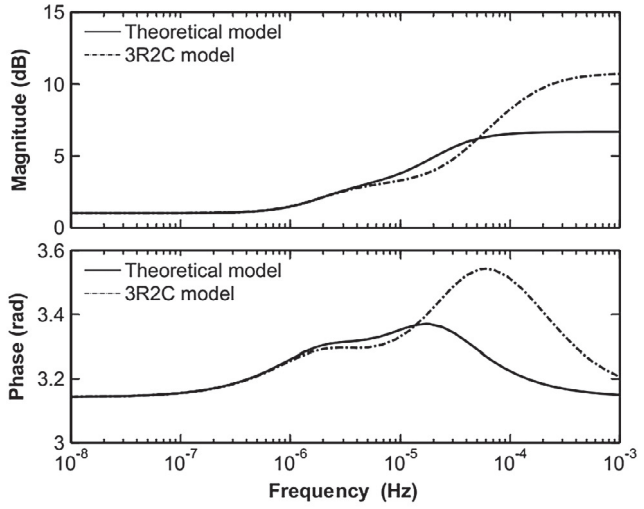

(a) External heat conduction

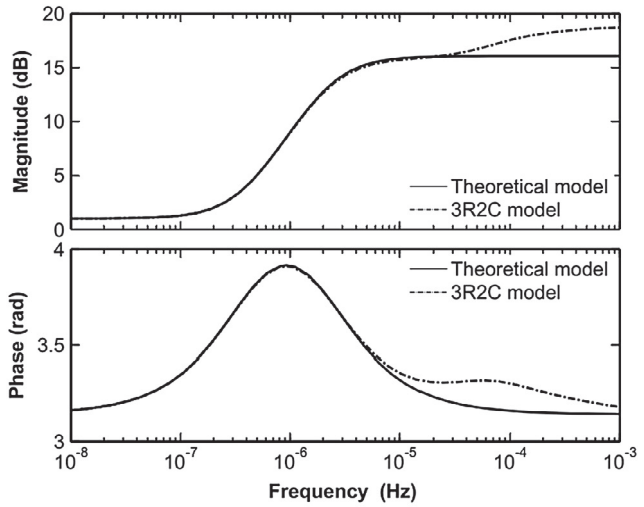

(b) Cross heat conduction

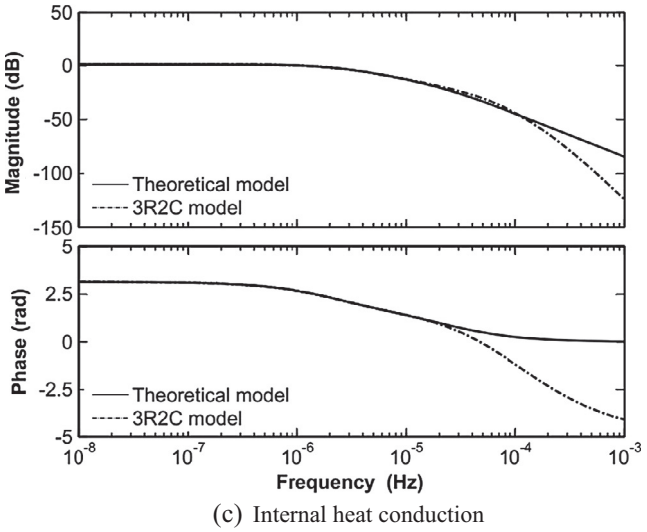

(c) Internal heat conduction

Fig. 9. Bode diagrams of roof.

5. Comparison of improved RC models

This section consists of three parts. Section 5.1 details the model parameter process for the building envelope and analyzes the modeling result. Monitored operating data and simulated data are both used to compare and validate four models in Sections 5.2 and 5.3.

5.1. Building envelope RC models

Based on the theory discussed in Section 3.2, a GA is utilized to conduct the non-linear parameter identification of the 3R2C model for the building external envelope (external walls and roofs). With a GA estimator, the R and C can be determined and the frequency response characteristic of the simplified model is then made to agree with that of the theoretical model. The simplified 3R2C model of the building envelope is calibrated with the real operations data. The detailed physical property parameters are tabulated in Table 6. The nodal placement of 3R2C models is listed in Table 7.

As depicted by the Bode diagrams in Fig. 8, the frequency characteristics of external, cross and internal heat conduction of the external wall are displayed for both the 3R2C model and the physical model. Similarly, Fig. 9 compares the frequency and phase lag characteristics of the roofs for the two models. Figs. 8(a) and 9(a) show that the RC model matches with the theoretical physical model in amplitudes and phase lags of the external heat conduction for the external walls. For the roofs, the two models have similar characteristics in the low frequency region, but there is a large bias in the high frequency region. However, the previous research indicated that the heat transfers from cross and internal conduction have a more considerable effect than those from the external heat conduction [38]. For cross heat conduction in both external walls and roofs, as shown in Figs. 8(b) and 9(b), the amplitudes and phase lags of the simplified model agree well with those of the theoretical model. In the internal heat conduction process, the simplified mode almost overlaps in the low and medium frequency regions and produces little deviation from the frequency responses of the theoretical model in the high frequency region (see Figs. 8(c) and 9(c)).

Fig. 10 presents the heat gains profile calculated by the theoretical model against that calculated by the simplified model for external walls and roofs. It can be seen that the simplified model has acceptable accuracy. The mean relative error between the two models is 8.8% for the external wall and 7.9% for the roof using Eq. (22).

$$\mathrm{MRE} = \frac{\sum_{k=1}^{N} \left| Q_{act,k} - Q_{est,k} \right|}{\sum_{k=1}^{N} \left| Q_{act,k} \right|} \tag{22}$$

where Q_{act} is the heat gain calculated by the theoretical model at the kth data point (kW). Q_{est} is the heat gain calculated by the simplified model at the kth data point (kW). N is the total number of data points.

5.2. Internal mass RC model compared to measured data

To further validate the simplified model of the building internal mass, a GA is still adopted as the efficient optimization means. The description can be found in Section 3.3. The parameter identification of the internal mass model is realized by figuring out the optimal values of R and C, which allows the predicted cooling load to best fit the measured cooling load.

The building thermal mass includes floor slabs, heavy interior load-bearing walls, lightweight partitions and a host of furniture and interior decorations. The area of the interior walls and floor slabs can be estimated with a small margin of error, but it is difficult to estimate the area of the remaining thermal mass. Thus, the search scope of R and C should be extended. In this paper, the upper limit of the R value is defined as the sum of resistances of the indoor air film and three times the resistance of the material. The upper limit of the C value is three times the capacitance of the material. The lower limit of both values is zero. The capacitance of the air is neglected in the calculation.

The measured operations data are selected for the parameter optimization process. The data acquisition and usage are explained in Section 4.2.2. The climate parameters are collected from a small

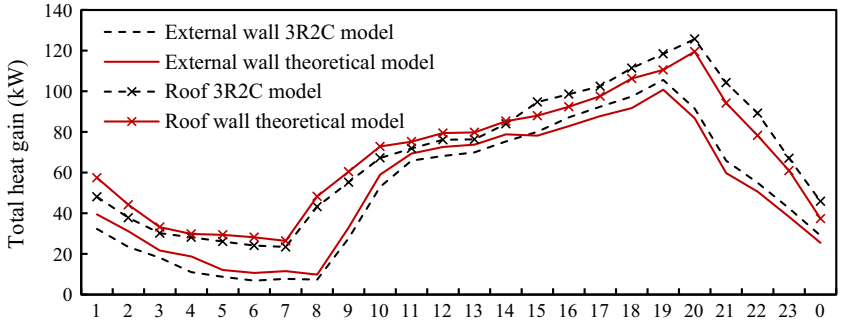

Fig. 10. Hourly heat gain through external wall and roof.

Table 8
Parameters of simplified internal mass models with on-site data.

Model No.	Parameters R (m^2 K/W)	Parameters C (MJ/(m^2 K))	MRE (%)
Model 0	$R_{im,1} = 0.0100$ $R_{im,2} = 0.0325$	$C_{im,1} = 5.9938$ $C_{im,2} = 1.9787$	16.57
Model 1	$R_{im,11} = 0.9586$ $R_{im,12} = 0.3794$ $R_{im,13} = 0.2617$	$C_{im,11} = 0.0175$ $C_{im,12} = 0.0276$ $C_{im,13} = 0.2968$	13.04
Model 2	$R_{im,21} = R_{im,22} = R_{im,23} = 0.4217$	$C_{im,21} = C_{im,22} = C_{im,23} = 0.1822$	12.15
Model 3	$R_{im,31} = R_{im,33} = 0.6560$ $R_{im,32} = R_{im,34} = 0.3431$ $R_{im,35} = 0.1291$ $R_{im,36} = 0.5290$	$C_{im,31} = C_{im,33} = 0.0288$ $C_{im,32} = C_{im,34} = 1.9964$ $C_{im,35} = 0.1947$ $C_{im,36} = 0.9592$	12.25

weather station and the specific weather data are shown in Fig. 4 in Section 4.2. The measured hourly cooling load ranges from Aug. 15th to Sep. 30th, 2014, and data from Aug 29th and 31st are missing. Thus, data from Aug. 16th to 28th are selected for training the four internal mass models. The hourly cooling load in September is calculated by the trained models and compared to the actual measured cooling load. MRE is calculated for all four models and the optimal parameter results are shown in Table 8.

Fig. 8 shows that the original model is the least accurate, and the three modified models predict the cooling load trend better than model 0. Model 2 is the best of the three improved models. Fig. 11 illustrates the comparison of the model 2 predicted cooling loads and the actual measured cooling load.

5.3. Internal mass RC model compared to physical model simulated data

The comparison of internal mass RC models is identical to the section above. Physical model simulated data rather than measured operations data are used to determine which RC model works best. The simulation model and the calibration process are described in Section 4.2.3. The simulated data for June is selected for the parameter optimization and three months of data in July, August and September are used for the estimation of the cooling load. By comparing the RC calculated cooling load to the simulated cooling loads, MREs are calculated for the four models. The result of the parameter identification and model validation is summarized in Table 9.

It can be concluded from Table 9 that model 0 is the least accurate. The three modified models are better than model 0 in terms of robustness and accuracy, and model 1 is the best. Fig. 12 demonstrates that the simplified model 1 can accurately predict the building dynamic thermal performance.

5.4. Analysis of results

The validation of the simplified models of the building envelope and thermal mass are demonstrated in the previous three Sections 5.1,5.2,5.3. In this section, the results of comparing four models are further discussed and analyzed. Using both measured operations data and physical model simulation data, the results confirm that model 0 (2R2C model for building internal mass) is the least accurate in predicting the building cooling load. In terms of robustness and accuracy, model 2 is more suitable with measured data and model 1 has the best match with physical model simulated data.

These results can be explained by the following assumptions: (1) It is assumed that the radiation heat distributes evenly on each surface in EnergyPlus, leading to a uniform temperature for each surface, which is not the case in reality. The sunlight irradiates floors through windows, and the temperature of the floor in sunlight is obviously higher than that of the shaded portion. This phenomenon explains why the RC model trained with operations data is sensitive to the distribution of the radiation while the physical model using the simulated data is not sensitive to it. (2) The internal temperature of the building internal mass is considered to be uniform in EnergyPlus; that is, the surface temperature is consistent with the internal temperature. As a result, the entire internal mass is involved in calculating the building cooling load. However, when considering heavyweight thermal mass in practice, such as some thick bearing walls, only the surface portion has an impact on the building loads. Thus, the RC model trained by the measured data is not very sensitive to the classification of thermal mass, while the model trained by EnergyPlus simulated data is sensitive to the classification.

The above discussion can explain why model 3 has an average performance in the two optimization processes. The hybrid RC model with parallel-connected after serial-connected masses is adopted based on consideration of the inhomogeneous temperature

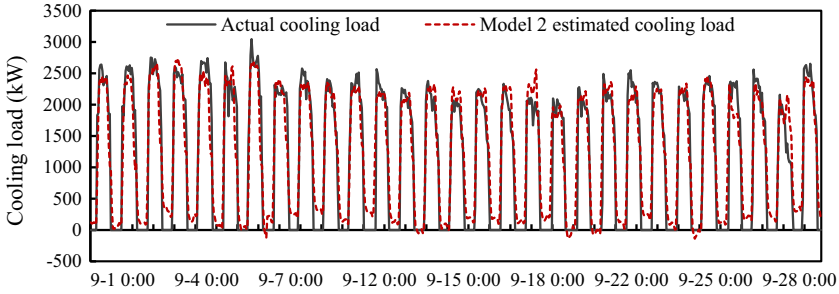

Fig. 11. Actual measured hourly cooling load vs model-predicted hourly cooling load (model 2).

Table 9
Parameters of simplified internal mass models with simulated data.

Model no.	Parameters R (m^2 K/W)	Parameters C (MJ/(m^2 K))	MRE (%)
Model 0	$R_{im,1} = 0.1576$ $R_{im,2} = 0.0289$	$C_{im,1} = 1.7491$ $C_{im,2} = 0.3883$	16.83
Model 1	$R_{im,11} = 0.2751$ $R_{im,12} = 0.1620$ $R_{im,13} = 0.9562$	$C_{im,11} = 0.0387$ $C_{im,12} = 0.0265$ $C_{im,13} = 0.2444$	9.50
Model 2	$R_{im,21} = R_{im,22} = R_{im,23} = 0.6251$	$C_{im,21} = C_{im,22} = C_{im,23} = 0.0148$	11.35
Model 3	$R_{im,31} = R_{im,33} = 1.9613$ $R_{im,32} = R_{im,34} = 1.0950$ $R_{im,35} = 1.8844$ $R_{im,36} = 0.4764$	$C_{im,31} = C_{im,33} = 0.6717$ $C_{im,32} = C_{im,34} = 0.3791$ $C_{im,35} = 0.6686$ $C_{im,36} = 0.1944$	11.60

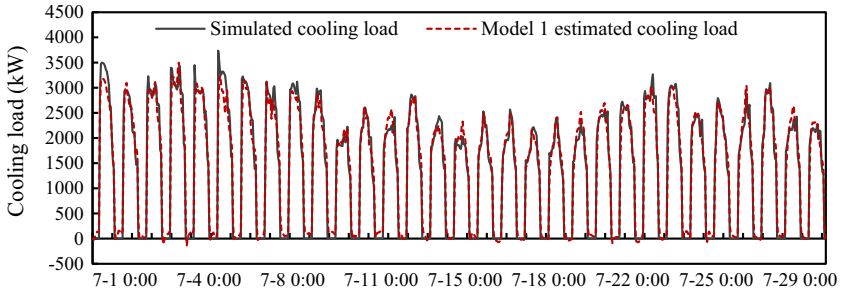

Fig. 12. Simulated hourly cooling load vs model-predicted hourly cooling load (model 1).

distribution of the internal mass. In the simulation group, model 3 is apparently not as good as model 1 due to the conditional assumption made in EnergyPlus. However, from the optimization result using the real operations data, model 3 is still not superior to other models. Thus, there is no need to use a complicated model (model 3) and a 3R3C parallel model (model 2) is sufficient to model the building internal mass.

6. Conclusions

Building upon the previous research on RC models, this study develops three improved RC-S models for calculating building cooling loads. Measured electricity submetering data are added to the model to calculate the internal heat gain from lighting and equipment. The RC-S model is a combination of a simplified 3R2C model for the building envelope, a simplified model for the building internal mass and an internal cooling load model based on submetering data. The accuracy of the RC-S model in estimating the cooling load is much better than traditional RC models. Compared to measured cooling load data in the case study, the best model is model 2, with a MRE of 12.15%. Compared to physical model simulated data, the best model is model 1, with a MRE of 9.50%.

We draw the following conclusions from this study. The simplified 3R2C model is fairly accurate for calculating the cooling load caused by the heat transfer of external walls and roofs. However, the 3R2C model is not good enough for calculating internal mass and internal heat gain. Three improved models proposed in this paper are all better than the baseline model (model 0) in predicting the cooling load. The comparison to the measured cooling load study demonstrated that the model accuracy is sensitive to the distribution of the solar radiation rather than the classification of thermal mass. Model 2 is the best model for estimating building cooling load in reality. However, the comparison result in the simulation data group is less sensitive to the distribution of the radiation than the classification of thermal mass. Therefore, the calculation result of model 1 is the closest to that of the EnergyPlus physical model simulation. The simplified 3R3C parallel model is sufficient to model the building internal mass and a more complex model configuration does not demonstrate better performance.

The case study has demonstrated the feasibility and applicability of the proposed "RC-S" method. To expand the application and improve its efficiency, the methodology in this paper will be made into a prototype toolkit for hourly building cooling load calculation in future studies. And this toolkit can also be integrated in HVAC system control, optimization or energy efficiency diagnosis platform.

References

[1] Key World Energy Statistics. IEA; 2009.
[2] US Department of Energy. 2010 Buildings Energy Data Book; 2010.
[3] Council EPA. Directive 2010/31/EU of the European parliament and of the council of 19 May, 2010 on the energy performance of buildings. Off J Eur Union 2010:13–35.
[4] Building energy conservation research center of Tsinghua University. Annual report on China building energy efficiency; 2013.
[5] Hong Taehoon, Koo Choongwan, Kim Jimin, Lee Minhyun, Jeong Kwangbok. A review on sustainable construction management strategies for monitoring, diagnosing, and retrofitting the building's dynamic energy performance: focused on the operation and maintenance phase. Appl Energy 2015;155:671–707.
[6] House J, Kelly G, (NIST). An overview of building diagnostic; 1999. <http://poet.lbl.gov/diag-workshop/proceedings>.
[7] Liu M, Song L, Claridge D, et al. Development of wholebuilding fault detection methods; 2002. <http://buildings.lbl.gov/hpcbs/pubs/E5P23T1c.pdf>.
[8] Handbook of fundamentals. American Society of Heating, Refrigerating and Air-Conditioning Engineers, Atlanta, USA; 2001.
[9] Karlsson F, Rohdin P, Persson ML. Measured and predicted energy demand of a low energy building: important aspects when using building energy simulation. Buil Serv Eng Res Technol 2007;28:223–35.
[10] Zhou YP, Wu JY, Wang RZ, Shiochi S, Li YM. Simulation and experimental validation of the variable-refrigerant-volume (VRV) air-conditioning system in EnergyPlus. Energy Build 2008;40(6):1041–7.
[11] Al-Ajmi FF, Hanby VI. Simulation of energy consumption for Kuwaiti domestic buildings. Energy Build 2008;40(6):1101–9.
[12] Coakley D, Raftery P, Keane M, Keane Marcus. A review of methods to match building energy simulation models to measured data. Renew Sustain Energy Rev 2014;37:123–41.
[13] Mustafaraj G, Marini D, Costa A, Keane M. Model calibration for building energy efficiency simulation. Appl Energy 2014;130:72–85.
[14] Yang Z, Becerik-Gerber B. A model calibration framework for simultaneous multi-level building energy simulation. Appl Energy 2015;149:415–31.
[15] Catalina T, Virgone J, Blanco E. Development and validation of regression models to predict monthly heating demand for residential buildings. Energy Build 2008;40(10):1825–32.
[16] Braun MR, Altan H, Beck SBM. Using regression analysis to predict the future energy consumption of a supermarket in the UK. Appl Energy 2014;130:305–13.
[17] Vaghefi A, Jafari MA, Bisse E, Lu Y, Brouwer J. Modeling and forecasting of cooling and electricity load demand. Appl Energy 2014;136:186–96.
[18] Ben-Nakhi AE, Mahmoud MA. Cooling load prediction for buildings using general regression neural networks. Energy Convers Manage 2004;45:2127–41.
[19] Gonzalez PA, Zamarreno JM. Prediction of hourly energy consumption in buildings based on a feedback artificial neural network. Energy Build 2005;37(6):595–601.
[20] Hou Z, Lian Z, Yao Y, Yuan X. Cooling-load prediction by the combination of rough set theory and an artificial neural-network based on data-fusion technique. Appl Energy 2006;83:1033–46.
[21] Ekici BB, Aksoy UT. Prediction of building energy consumption by using artificial neural networks. Adv Eng Softw 2009;40(5):356–62.
[22] Li Q, Meng Q, Cai J, Yoshino H, Mochida A. Applying support vector machine to predict hourly cooling load in the building. Appl Energy 2009;86(10):2249–56.
[23] Hou Z, Lian Z. An application of support vector machines in cooling load prediction. Int Syst Application ISA 2009;5:1–4.
[24] Protić M, Shamshirband S, Petković D, et al. Forecasting of consumers heat load in district heating systems using the support vector machine with a discrete wavelet transform algorithm. Energy 2015;87:343–51.
[25] Wehenkel L, Pavella M. Decision tree approach to power systems security assessment. Int J Electr Power Energy Syst 1993;15(1):13–36.
[26] Yu Z, Haghighat F, Fung BCM, Yoshino H. A decision tree method for building energy demand modeling. Energy Build 2010;42:1637–46.
[27] Dhar A, Reddy TA, Claridge DE. Generalization of the Fourier series approach to model hourly energy use in commercial buildings. ASME J Sol Energy Eng 1999;121(1):54–62.
[28] Dhar A, Reddy TA, Claridge DE. A Fourier series model to predict hourly heating and cooling energy use in commercial buildings with outdoor temperature as the only weather variable. ASME J Sol Energy Eng 1999;121(1):47–53.
[29] Dhar A, Reddy TA, Claridge DE. Generalization of the Fourier series approach to model hourly energy use in commercial buildings. Trans ASME 1999;121:54.

[30] Kreider JF, Rabl A, Curtiss P. Heating and cooling of buildings: design for efficiency. McGraw-Hill, Inc.; 1994.
[31] Braun K, Chaturvedi N. An inverse gray-box model for transient building load prediction. HVAC&R Res 2002;8(1):73–99.
[32] Liao Z, Dexter AL. A simplified physical model for estimating the average air temperature in multi-zone heating systems. Build Environ 2004;39:1013–22.
[33] Mitchell M. An introduction to genetic algorithm. Cambridge (MA): MIT Press; 1997.
[34] Seem JE, Beckman WA, Klein SA, et al. Transfer functions for efficient calculation of multidimensional transient heat transfer. J Heat Transf 1989;11:5–12.
[35] Xu X, Wang S. A simplified dynamic model for existing buildings using CTF and thermal network models. Int J Therm Sci 2008;47:1249–62.
[36] Xu X, Wang S. Optimal simplified thermal models of building envelope based on frequency domain regression using genetic algorithm. Energy Build 2007;39:525–36.
[37] Wang S, Xu X. Parameter estimation of internal thermal mass of building dynamic models using genetic algorithm. Energy Convers Manage 2006;47:1927–41.
[38] Wang S, Xu X. Simplified building model for transient thermal performance estimation using GA-based parameter identification. Int J Therm Sci 2006;45:419–32.
[39] Kusuda T. Thermal response factors for multilayer structures of various heat conduction systems. ASHRAE Trans 1969;75:246–71.
[40] Ouyang K, Haghighat F. A procedure for calculating thermal response factors of multilayer walls—state space method. Build Environ 1991;26(2):173–7.
[41] Ciampi M, Leccese F, Tuoni G. Multi-layered walls design to optimize building-plant interaction. Int J Therm Sci 2004;43(4):417–29.
[42] Chen YM, Chen ZK. A neural-network-based experimental technique for determining z-transfer function coefficients of a building envelope. Build Environ 2000;35:181–9.
[43] Wang S, Chen Y. A novel and simple building load calculation model for building and system dynamic simulation. Appl Therm Eng 2001;21:683–702.
[44] Handbook of fundamentals. American Society of Heating, Refrigerating and Air-Conditioning Engineers, Atlanta, USA; 2005.
[45] Emmerich SJ, Persily AK. Energy impacts of infiltration and ventilation in US office buildings using multizone airflow simulation. Proc IAQ Energy 1998;98:191–206.
[46] Ng LC, Persily AK, Emmerich SJ. Improving infiltration modeling in commercial building energy models. Energy Build 2015;88:316–23.
[47] Sandberg M, Mattsson M, Wigö H, Hayati A, Claesson L, Linden E, et al. Viewpoints on wind and air infiltration phenomena at buildings illustrated by field and model studies. Build Environ 2015;92:504–17.
[48] Ji Y, Xu P, Ye Y, Yunyang Ye. HVAC terminal hourly end-use disaggregation in commercial buildings with Fourier series model. Energy Build 2015;97:33–46.
[49] Ji Y, Xu P. A bottom-up and procedural calibration method for building energy simulation models based on hourly electricity submetering data. Energy 2015;93:2337–50.